Mycobacterial OtsA structures reveal an allosteric site regulated by 2-oxoglutarate and 2-phosphoglycerate and the mechanism for substrate preference.

Vítor Mendes[1*], Marta Acebrón-García-de-Eulate[1], Nupur Verma[1], Michal Blaszczyk[1], Márcio V. B. Dias[2,3] and Tom L. Blundell[1*]

1 - Department of Biochemistry, University of Cambridge, Cambridge CB21GA, UK.

2 - Department of Microbiology, Institute of Biomedical Science, University of São Paulo, São Paulo, Brazil.

3 – Department of Chemistry, University of Warwick, Coventry CV4 7EQ, UK.

*Corresponding authors

Tom L. Blundell

Address: Department of Biochemistry, University of Cambridge, 80 Tennis Court Road, CB2 1GA Cambridge, UK.

Phone: +441223333628

Email: tom@cryst.bioc.cam.ac.uk

Vitor Mendes

Address: Department of Biochemistry, University of Cambridge, 80 Tennis Court Road, CB2 1GA Cambridge, UK.

Phone: +441223766028

Email: vgm23@cam.ac.uk

Abstract

Trehalose is an essential disaccharide for mycobacteria and a key constituent of several cell wall glycolipids with fundamental roles in pathogenesis. Mycobacteria possess two pathways for trehalose biosynthesis. However, only the OtsAB pathway was found to be essential in *M. tuberculosis*, with marked growth and virulence defects of OtsA mutants and strict essentiality of OtsB2. Herein, we report here the first mycobacterial OtsA structures from *M. thermoresistibile* in both apo and ligand-bound forms. Structural information reveals three key residues in the mechanism of substrate preference that were further confirmed by site-directed mutagenesis. Additionally, we identify 2-oxoglutarate and 2-phosphoglycerate as allosteric regulators of OtsA. The structural analysis in this work strongly contributed to define the mechanisms for feedback inhibition, show different conformational states of the enzyme and map a new allosteric site.

Introduction

Trehalose is a non-reducing disaccharide, formed by α-(1-1) linked glucoses, with a wide distribution in nature and present in all three domains of life (1). This remarkably widespread sugar performs multiple roles in a wide variety of organisms and it can also fulfil different roles within the same organism. Trehalose has been considered a compatible solute, conferring protection to proteins, DNA, membranes and whole cells from thermal shock, osmotic shock, freezing, ionizing radiation, oxidative stress and desiccation (1-9). This disaccharide, which can further function as a carbon and energy reserve molecule (1, 10-12), was also recently related to pathogenicity of *Pseudomonas aeruginosa* in plants (13). It additionally plays fundamental signaling roles in plants in the phosphorylated form (trehalose-6-phosphate) where it regulates sucrose metabolism and flowering (1, 14-16) and in yeast where it regulates gluconeogenesis and glycolysis (17, 18). Trehalose was further shown to be an autophagy inducer, both in plants and in mammals, with potential biotechnological and clinical implications (19, 20).

In mycobacteria, trehalose is also an essential component of mycolic acids, which are major protagonists in *Mycobacterium tuberculosis* pathogenesis (1, 21), the causative agent of the widespread infectious disease tuberculosis. In these organisms, trehalose was further identified as a key signaling molecule of cell-envelope stress playing a role as an activator of the iniBAC operon, which is induced when mycobacteria are exposed to the first line drug isoniazid (22).

All mycobacterial species, with a few exceptions, possess two pathways to synthesize trehalose, the OtsAB and the TreYZ pathway (1). The OtsAB pathway is the most widely distributed trehalose biosynthesis pathway, present in bacteria, archaea and eukaryotes (23, 24). In this pathway, which is conserved and essential in mycobacteria, trehalose is

synthesized in a two-step process involving OtsA and OtsB2 enzymes. *M. tuberculosis* mutants showed that the OtsAB pathway was not only the dominant route for trehalose biosynthesis in this pathogen but also required for growth both *in vitro* and in a mouse infection model, with marked growth and virulence defects of OtsA mutants (25) and strict essentiality of OtsB2 due to the toxic effect of trehalose-6-phosphate (T6P) accumulation (25, 26).

OtsA, a glycosyltransferase that belongs to the GT20 family of the CAZY classification (www.cazy.org), uses the α anomer of glucose-6-phosphate (G6P) as acceptor and NDP-glucose as the donor to synthesize T6P, with net retention of the anomeric configuration of the donor substrate (27, 28). Interestingly, OtsAs from different organisms show different donor preferences as shown by kinetic studies and X-ray crystal structures, but the reasons behind these preferences are poorly understood (28-33). Recently, different roles were identified for OtsA beyond its enzymatic activity. OtsA was reported to act as an osmotic stress sensor and morphogenetic protein that can regulate the switch to myceloid growth in *Arthrobacter sp.* strain A3, a pleomorphic soil dwelling actinobacteria (34).

In this work we have purified, crystallized and solved the structure of *Mycobacterium thermoresistibile* OtsA (*Mtr*OtsA). To gain further insight into mycobacterial OtsA, we have obtained structures with substrates, product and pathway product that offer insight for mechanisms of substrate preference and feedback inhibition. We further performed structure-guided point mutations of key residues and characterized the mutants showing that three mutations are enough to change substrate preference. Importantly with these structures, we have also identified a new allosteric site and novel allosteric regulators of this enzyme that link glycolytic and TCA cycle metabolites to the regulation of "*de novo*" trehalose synthesis.

Results

Overall structure

*Mtr*OtsA is composed of two Rossmann-fold domains with a deep catalytic site at their interface, in an arrangement typical of GT-B glycosyltransferases as described previously for other organisms (28-30). The apo protein crystallized in the $I4_122$ space group, with one protomer per asymmetric unit, and diffracted to ~1.8 Å resolution. The N-terminal domain is formed by a core of 7 parallel strands flanked on both sides by an antiparallel strand and surrounded by 8 α-helixes, one of which is composed of the final C-terminal residues (Fig. 1A). The C-terminal domain contains 6 parallel stands associated with 9 α-helixes with the last one undergoing a kink and extending to the N-terminal domain (Fig 1A). Analysis of the B-factor distribution shows that the N-terminal domain has the highest values for atomic temperature factors, suggesting that this domain is more dynamic, which is consistent with the large movements of α-1 during catalytic activity.

*Mtr*OtsA forms a tetramer in solution, as previously observed for *M. tuberculosis* OtsA. This tetrameric form is also observed in all the crystal structures reported herein (Fig 1B). The amino acids involved in the tetramer interfaces are not conserved beyond mycobacteria and related species (Fig S1), suggesting that OtsA might have a different molecular assembly in different species. Indeed in *E. coli* both tetrameric and dimeric forms were reported (28) and in *Streptomyces venezuelae*, *Aspergillus fumigatus* and *Candida albicans* only the dimeric form was observed (29, 30). However, in mycobacteria and closely related organisms the tetramer interfaces are highly conserved, suggesting a tetrameric assembly of OtsA in all of these organisms (Supplementary Fig S1).

Catalytic site

OtsA, is a glycosyltransferase that uses the α anomer of G6P as acceptor and NDP-glucose as the donor to synthesize T6P. The *Mtr*OtsA catalytic site is located between the two Rossmann-fold domains in a large and deep cavity. Structures with donor substrates were determined by soaking the apo form crystals with ADP-glucose and GDP-glucose (Fig 2). The donor substrates interact primarily with the C-terminal domain through the side chains of the highly conserved Arg286, Lys 291, Asp385, Glu393 and with the side chain of Arg365 (Fig 2), which is conserved in all mycobacteria and closely related species but less conserved outside this group (Fig S1). Backbone interactions with the absolutely conserved residues Gly386, Met387 and Leu389 amine groups are also observed. N-terminal domain interactions with the donor substrate are only observed for His168 when the active site is in an open conformation (Fig 2). To obtain a structure with the acceptor substrate, we co-crystallized OtsA in the presence of 5 mM ADP and G6P. As G6P binds to the protein in the presence of a donor substrate or its nucleotide, the active site adopts to a closed conformation (Fig 3A). The OtsA:ADP:G6P ternary complex crystallized in the $P6_222$ space group, with one protomer per asymmetric unit, and the crystals diffracted up to ~1.7 Å resolution. In this closed conformation new interactions with the donor substrate are formed with the side chain of Thr42 and the Gly39 peptide-NH function (Fig 3). Due to the absolute conserved nature of Gly39 and the contact it forms with the glucose-bound phosphate, this residue is highly likely to be mechanistically involved in the catalytic activity as proposed before (28).

The acceptor substrate interacts with the highly conserved residues Arg18, Tyr90, Asp144 and Gln146 of the N-terminal domain and with only a single residue of the C-

terminal domain, Arg324 (Fig 3B). The residues involved in acceptor substrate interaction are highly conserved in all species (Fig S1). As described for *E. coli* OtsA (28), the OtsA:ADP:G6P ternary structure shows the catalytic site in a closed conformation that substantially differs from the apo form, with α-helix 1 and the Arg35-Gly39 loop region moving up to ~12 Å (Fig 3A).

Properties of *M. thermoresistibile* OtsA.

*Mtr*OtsA uses ADP-glucose, UDP-glucose and GDP-glucose as glucose donors with decreasing efficiency (Table 1) and G6P as the only acceptor, in accordance to what was reported before for *M. tuberculosis* OtsA (33, 35). The kinetic parameters for *Mtr*OtsA were obtained and are reported in (Table 1) and (Fig. S2) with K_m values for preferred donor substrate (ADP-Glucose) of 0.25 ± 0.02 mM and for the acceptor (G6P) of 3.3 ± 0.1 mM. The K_m for GDP-glucose of 0.29 ± 0.02 mM was in the same range as the one obtained for ADP-glucose, however the turnover was 5 fold lower (Table 1). For UDP-glucose, the enzyme showed a ~7 fold higher K_m of 1.7 ± 0.1 mM than the one obtained for ADP-glucose (Table 1).

The preference of ADP-glucose over the other glucose donors was further confirmed by isothermal titration calorimetry (ITC). The binding affinity of substrate donors could only be determined for ADP-glucose in the tested conditions with an observable K_d of 27.17 μM ± 2.66 μM (Fig S3). Other glucose donors analysed (GDP-glucose and UDP-glucose) had no observable heat of binding and the same was observed for G6P. The lack of heat of binding for GDP- and UDP-glucose is most likely due to their reduced affinity. For G6P case, it reflects a necessity of previous binding of the donor substrate.

Donor substrate preference is largely mediated by three residues

OtsAs from different organisms have been shown to have different donor substrate preferences, while being capable of using several nucleotide donors (30, 33, 36, 37), which is reflected in lower conservation of the donor substrate interacting residues (Fig S1). Preference for ADP-glucose as the donor substrate in *Mtr*OtsA is conferred by interactions with the deeply buried adenine moiety (Fig 4A). The carbonyl groups of Leu319 and Arg361 interact with the primary amine, and the amide group of Val363 interacts with N1 of the adenine moiety (Fig 4A). A highly coordinated water is also interacting with the primary amine of the adenine moiety and the carbonyl groups of Ala320, Leu359 and Arg361. The guanine moiety of GDP-glucose cannot occupy the same deeply buried pocket as the adenine because its primary amine group would sterically clash with Val363 carbonyl group (Fig 4B). It thus binds to OtsA more weakly than ADP-glucose explaining the substrate preference and consequently the lack of observable heat of binding in the tested ITC conditions. A binary complex structure with OtsA and UDP-glucose was also obtained but the electron density was only observed for glucose and the two phosphates (not shown) indicating a reduced preference for this substrate as confirmed by enzymatic and biophysical data. Comparing mycobacterial OtsAs with *E. coli*, we hypothesised that the ADP preference was mediated by the substitution of an isoleucine (Ile295 in *E. coli*) for a leucine (Leu319 in *M. thermoresistibile*) that allows the primary amine of the adenine moiety to occupy a buried position interacting with the carbonyl group of Leu319 (Fig 4C) that no other nucleotide activated donor can occupy. However, given the residue differences between the two enzymes it is likely that other residues could also play a role. To improve the selection of residues to mutate we employed a computational approach by using a mCSM-lig (38), a software developed by our group that predicts the effects of mutations on binding affinity. The software predicted several that residues within 4.5 Å of the adenine moiety have a

destabilizing effect on the interaction with the ligand if mutated to the *E. coli* OtsA equivalent (Table S2). Combining this information with structural analysis we selected three mutations predicted to be destabilizing; Val363Phe, Leu319Ile and Glu367Leu, the latter being a long distance mutation that we hypothesised would have a strong effect on ligand binding.

To confirm our hypothesis, we generated several *Mtr*OtsA mutants (Leu319Ile, Val363Phe, Leu319Ile-Glu367Leu and a triple mutant) and we obtained kinetic properties for all of them (Table 1). As we predicted the mutant Leu319Ile showed a ~3 fold increase e in the K_m for ADP-glucose whereas, K_m was similar GDP-glucose and UDP-glucose when compared to the wild type. Even though GDP-glucose now showed the best K_m among the three different donors, the catalytic efficiency and turnover rate was still higher for ADP-glucose (Table 1). A complete reversal of the donor substrate preference for UDP-glucose was obtained only with a combination of the three mutations (Table 1). The triple mutant showed a ~5 fold increase in ADP-glucose K_m and a reduction for the UDP-glucose K_m by more than 3 fold (Table 1). The catalytic efficiency was also completely reversed for ADP- and UDP-glucose between the wild-type and the triple mutant (Table 1). Although Leu319Ile showed the largest contribution for ADP-glucose K_m increase, Val363Phe and Glu367Leu were also determinant for the reversal to UDP-Glucose preference (Table 1). This can be explained by the fact that the phenylalanine substitution at position 363 forces the loop between β-14 and α-14 to move towards the nucleotide binding site (Fig 4C), thus establishing stronger interactions with a pyrimidine nucleotide and clashing with purine ones. This effect is also observed for both ADP- and GDP-glucose, with a ~2.5 fold increase in K_m when compared to the wild type. The leucine substitution at position 367 further helps in this move since the hydrogen bonds

between the side chains of Arg266 and Glu367 are no longer present and α-14 is repelled from Arg266 due to the Leu side chain (Fig 4C).

Feedback inhibition

We soaked both trehalose and T6P into apo OtsA crystals and solved structures with both ligands (Fig 4D and 4E). In both structures OtsA active site assumes an open conformation and two compounds superpose almost perfectly at active site, recapitulating all of the interactions for the donor glucose and also interacting with His199 and Arg286, the latter a residue that interacts with the phosphates of the donor substrate (Fig 4D and 4E). The structure with T6P further shows the phosphate group of the product occupying a similar position to the phosphate group of G6P, interacting with the side chains of Tyr90, Gln146, Arg324 and Tyr145 a residue that does not interact with G6P (Fig 4E). Interestingly the buffer present in the crystallization condition (CHES) is observed in both trehalose and trehalose-6-phosphate bound structures, occupying the site of the nucleotide donor with the sulphate group binding in a phosphate site and interacting with hydroxyl groups from both glucose units of trehalose (Fig 4D and 4E).

After obtaining these structures, it was expected to observe some degree of feedback inhibition of OtsA by both trehalose and T6P. Both trehalose-6-phosphate and trehalose inhibited the enzyme, but the effect of trehalose was more pronounced with ~40% inhibition at 10 mM while for trehalose-6-phosphate a maximum inhibition of ~25% was reached at the same concentration (Fig S4). These results show that under physiological conditions OtsA is regulated by trehalose, the final product of the pathway which is highly abundant inside mycobacterial cells, but not by T6P which is known to be toxic for cells at high concentrations (26).

Identification of an allosteric site in *M. thermoresistible* OtsA

Trehalose is a multipurpose molecule that is abundant in mycobacteria. It can function not only as an energy reserve and as structural component of cell wall glycolipids, but can also lead to the synthesis of glycogen through the TreS-Mak-GlgE pathway and be directly synthesised from glycogen. It is therefore likely that "*de novo*" trehalose synthesis is under strong regulation.

In all the crystallization conditions that contained CHES, we could observe this compound in the crystal structures occupying a pocket formed by the contact interface of 2 OtsA protomers in the tetrameric assembly (Fig 5). The CHES sulphate group directly interacts with the side chains of Arg384 of protomer A and Arg213 of protomer B, forming hydrogen bonds with both, but also hydrophobic hydrogen-π interactions with Phe410 of protomer A (Fig 5). The residues composing this site are completely conserved in mycobacterial and closely related species that are likely to arbour OtsA tetramers but not on others species known to have other oligomeric forms (Fig S1).

Arg384 sits in a loop that forms extensive contacts with the donor substrate through Asp385, Gly386, Met387 and Leu389 (Fig 2). Ligands interacting with the side chain of Arg384 could therefore have an impact on the activity of the enzyme making this site a prime candidate for allosteric regulation.

While CHES had no discernible impact on OtsA activity in the tested concentrations, it was reported before that F6P acted as an allosteric regulator of *M. tuberculosis* OtsA (35), and the same was reported for yeast OtsAB complex (39). We have tested *Mtr*OtsA in the same conditions as those reported by Diez and colleagues, and could not detect any effect of F6P for *Mtr*OtsA. Although we did not observe any effect of F6P on enzyme activity for *Mtr*OtsAs, we nevertheless attempted to soak this compound in both apo form and OtsA:ADP:G6P ternary complex crystals, and also co-crystallize it in the presence and

absence of ADP and G6P, all in CHES free conditions. None of these conditions provided a structure in which F6P occupied an allosteric site. We could however observe F6P when co-crystallized together with ADP, bound to the acceptor substrate site and occupying the G6P site, with OtsA presenting the active site in a closed conformation (Fig S5).

OtsA was found to interact with a multitude of proteins in a large-scale proteomics study (40), including enolase that catalyses the penultimate step of glycolysis. In our search for an allosteric regulator we, therefore, decided to test several glycolytic metabolites glucose-1-phosphate (G1P), fructose-1,6-biphosphate (F16BP), 3-phosphoglycerate (3PG), the enolase substrate 2-phosphoglyceric acid (2PG) and product phosphoenolpyruvate (PEP), but also the master metabolic regulators cAMP and 2-oxoglutarate (2OG) (41), and assess their impact in OtsA activity.

From the several compounds tested only 2OG and 2PG showed clear inhibition of OtsA activity with IC_{50} of 1.8 mM and 2.3 mM respectively (Table 2) and (Fig 5C). To assess whether they could be acting allosterically on *Mtr*OtsA and binding to the site identified by CHES we performed two mutations on the arginines that interacted with CHES (Arg213Glu and Arg384Glu) and tested the two mutants activity in the presence of 2OG and 2PG. The results show that the Arg213Glu mutation abolished the strong response of the protein to 2OG while there was a ~5 fold increase in 2PG IC_{50} to 12 mM. For the Arg384Glu mutant 2OG becomes unexpectedly becomes a strong activator with an EC_{50} of 0.7 mM while 2PG has no effect (Table 2).

Discussion

Trehalose, an essential disaccharide in mycobacteria, is one of the critical components of the cell wall. The OtsA-B pathway is an essential source of trehalose for these organisms with knock-outs of this pathway being highly defective or non-viable (25, 26). Here we

reveal the first mycobacterial OtsA structure. The overall structure of *M. thermoresistibile* OtsA is similar to the reported structures of *E. coli*, *S. venezuelae* and *Pseudoburkholderia xenovorans* OtsAs despite relatively low sequence identity (33 and 35% respectively). Remarkably, OtsAs have also a highly similar fold to the pseudo-glycosyltransferases VldE and ValL involved in validamycin A synthesis, a potent antifungal agent (42, 43). The structures obtained in this work allow us to explain how mycobacterial OtsA preference for ADP-glucose, is conferred by Leu319 which creates a cavity to accommodate the primary amine of the adenine moiety allowing it to interact with Leu319 and Arg361carbonyl groups. It is further mediated by Val363 carbonyl group that does not allow GDP-glucose to occupy the same position and Glu367. Mutating these three residues to the *E. coli* OtsA equivalents completely changed the preference to UDP-glucose, the preferred *E. coli* OtsA donor substrate.

Trehalose is not only abundant inside the mycobacterial cell but also involved in a cycle that links it to the synthesis and degradation of glycogen (44). We have shown that OtsA is feedback inhibited by trehalose but not by T6P even though the structures obtained show that both compounds form extensive interactions with OtsA. However, given that these two structures were obtained by soaking apo form crystals with high concentrations of trehalose and T6P, and that CHES is also observed at the active site interacting with both compounds, it is possible that these two structures do not entirely reflect their natural interactions with the enzyme.

Further regulation of players in these pathways has been reported for GlgE, an enzyme that links trehalose recycling to glycogen synthesis, and that is regulated by phosphorylation (45). OtsA regulation by phosphorylation and methylation has also been observed for yeast trehalose-6-phosphate synthase complex (46, 47). However, unlike yeasts that have several different OtsA genes forming a complex, bacteria only possess

one form of OtsA and there are no reports of regulation by phosphorylation of this enzyme in these organisms. Although, allosteric regulation mediated by F6P was reported for both *M. tuberculosis* and yeast OtsAs (35, 39), we could not find any F6P allosteric effect for *Mtr*OtsA despite testing several different assay conditions including those reported in the literature for *M. tuberculosis*, nor could we see F6P occupying the allosteric site in any of our structures irrespective of the methods and conditions used to obtain crystals. F6P was found however occupying the donor site when co-crystallized in the presence of ADP. The observed differences in regulation by F6P between mycobacterial enzymes are difficult to reconcile since the allosteric site is highly conserved in mycobacterial OtsAs and closely related species (supplementary Fig S1).

We could nevertheless observe in many of our structures CHES occupying a site between two protomers that due to the interactions formed with Arg384 could affect the activity of the enzyme (Fig 6). The reported interaction of OtsA with enolase (40) prompted us to test several glycolytic intermediates in our search for allosteric regulators, and we further included the metabolic regulators cAMP and 2OG. From the tested compounds only 2PG, the substrate of enolase, and 2OG had a regulatory effect of *Mtr*OtsA activity within relevant physiological concentrations (48, 49). Mutation of the allosteric-site residues Arg213 and Arg384 completely altered the effect of these allosteric inhibitors (Table 2), demonstrating that the compounds indeed act through the allosteric site. The Arg384 mutation that transforms 2OG an allosteric inhibitor in an activator of OtsA hints at the possibility of allosteric activators of OtsA, however that remains to be confirmed.

The reported interaction between enolase and the fact that its substrate 2PG acts as an allosteric regulator of OtsA shows an interplay between these two enzymes that would be interesting to explore further on the enolase side. Similarly the allosteric regulation by

2OG a molecule that sits at the interface of carbon and nitrogen metabolism and that has been shown to regulate many different pathways (41) demands further work.

The results of this work are a significant step forward in understanding the regulation of "*de novo*" trehalose synthesis in mycobacteria the structural reasons behind substrate preference, and provide new important insight into this enzyme.

Methods

Bacterial strains and cloning.

M. thermoresistibile (DSM 44167) *otsA* gene was amplified from chromosomal DNA obtained from the Deutsch Sammlung von Mikroorganismen und Zellkulturen GmbH (DSMZ, Braunschweig, Germany). Primers were designed based on the sequence available in NCBI database and the gene was cloned between the BamHI and HindIII sites in pET28a vector (Novagen), modified with an N-terminal 6xHis-SUMO tag. The resulting plasmid was confirmed by DNA sequencing and transformed into *E. coli* BL21(DE3) strain (Invitrogen). Six *Mtr*OtsA mutants (Arg213Glu, Leu319Ile, Val363Phe, Arg384Glu, Leu319Ile-Glu367Leu and Leu319Ile-Val363Phe-Glu367Leu) were also constructed by site-specific mutagenesis, sequenced and transformed into *E. coli* BL21(DE3) strain.

Recombinant expression and protein purification

Transformed *E. coli* BL21(DE3) cells were grown to mid-exponential growth phase (OD_{610} = 0.6) in LB media (Invitrogen) containing 30 mg L^{-1} kanamycin at 37 ºC. Isopropyl β–D-1-thiogalactopyranoside (IPTG) was then added at a final concentration of 0.5 mM to induce gene expression and the temperature was lowered to 18 ºC. Cells

were harvested 18 h-20 h later by centrifugation and re-suspended in 20 mM TRIS pH 7.5, 500 mM NaCl and 20 mM Imidazole with protease inhibitor tablets (Roche), DNAseI and 5 mM $MgCl_2$. Cells were lysed by sonication and cell lysate was centrifuged at 27000 g for 30 min to remove cell debris.

Recombinant *Mtr*OtsA was purified with a HiTrap IMAC Sepharose FF column (GE-Healthcare), equilibrated with 20 mM TRIS pH 7.5, 500 mM NaCl and 20 mM Imidazole. Elution was performed in the same buffer, but with 500 mM Imidazole. Imidazole was removed with a desalting column and SUMO tag was cleaved overnight at 4 ºC by adding Ulp1 protease at 1:100 ratio in 20 mM TRIS pH 7.5, 500 mM NaCl. SUMO tag, Ulp1 protease and uncleaved SUMO-OtsA were removed with a HiTrap IMAC Sepharose FF column (GE-Healthcare), equilibrated with 20 mM TRIS pH 7.5, 500 mM NaCl and 20 mM imidazole. Flow through containing OtsA was collected, concentrated and loaded to a Superdex 200 column equilibrated with 20 mM TRIS pH 7.5, 500 mM NaCl. Fraction purity was determined by SDS-page and purest fractions were pooled concentrated to ~10 $mg.ml^{-1}$ in 20 mM TRIS pH 7.5 350 mM NaCl, flash frozen in liquid nitrogen and stored at -80 ºC. The same purification protocol was used for all *Mtr*OtsA mutants.

Crystallization and data collection

*Mtr*OtsA crystallization screens and optimization were performed at 18 ºC using sitting-drop vapour diffusion method. 300 nl of pure OtsA at 10 $mg.ml^{-1}$ was mixed in 1:1 ratio with well solution using a Phoenix robot (Art Robbins). Initial conditions were obtained in classics suite crystallization screen (Qiagen), solution 36. Crystals obtained in this condition diffracted only up to 3 Å. Therefore, further optimization was performed using the additive screen HT (Hampton Research) and ethylene glycol was found to be the best additive. The final optimized condition consisted of 0.7 M sodium potassium tartrate, 0.1

M CHES pH 10 and 10% v/v ethylene glycol. Crystals appeared after 4 days in this condition. To obtain ligand-bound structures soaking was performed in the optimized condition using the hanging drop vapour diffusion method as follows: 1 µl of protein storage buffer containing 5 mM of ligand was mixed with 1 µl of reservoir solution and drops were left to equilibrate against 500 µl of reservoir solution for 3 days. Crystals were then transferred to the pre-equilibrated drops and incubated for 24h. A cryogenic solution was prepared by adding ethylene glycol up to 25% v/v to mother liquor. Crystals were briefly transferred to this solution, flash frozen in liquid nitrogen and stored for data collection. To obtain an ADP-G6P-OtsA ternary complex co-crystallization with 5mM ADP and G6P was performed instead, as all attempts to soak G6P alone or G6P in the presence of ADP have failed. Crystals were obtained in the Wizard Classic I&II screen (Rigaku), solution E10 and were flash frozen in liquid nitrogen after a brief soak in a solution containing mother liquor and 25% ethylene glycol. The same condition was used to obtain ADP:F6P:OtsA complex.

All data sets were collected at stations I04, I04-1 and I24 at Diamond Light Source (Oxford, UK). Data collection and refinement statistics are summarized in (Table S1).

Structure solution and refinement

Diffraction data were processed and reduced using MOSFLM (50) and Aimless (51) from the CCP4 suite (52), or autoPROC from Global Phasing Limited (53). The apo form crystalized in $I4_122$ space group with one protomer per asymmetric unit. ADP-G6P-OtsA ternary complex crystallized in $P6_222$ space group again with one protomer per asymmetric unit.

Initial phases were determined with PHASER (54) from PHENIX software package (55) using the structure of *E. coli* OtsA (PDB entry 1UQU) (32) as a search model. Model

building was done with Coot (56) and refinement was performed in PHENIX (55). Structure validation was performed using Coot and PHENIX tools (55, 56). All the figures were prepared with Pymol (http://www.pymol.org).

Prediction of mutations in ligand affinity

To provide an insight on which residues to mutate, we used mCSM-lig a software that predicts the effect of mutations in ligand affinity (38) on the X-ray crystal structure of OtsA with ADP-glucose (5JIO).

Enzymatic Assays

Formation of T6P was assessed by a continuous colorimetric assay that followed the release of NDP by measuring the oxidation of NADH at 340nm, in the presence of pyruvate kinase and lactate dehydrogenase. All reagents used were obtained from Sigma-Aldrich. The enzymatic reactions (200 µl) were performed at 37 ºC and contained 50 mM TRIS pH 7.5, 200 mM NaCl, 10 mM $MgCl_2$, 50 mM KCl, 0.3 mM NADH, 2.5 mM phosphoenolpyruvate (PEP), 10 units of pyruvate kinase/lactate dehydrogenase, 0.1 µM enzyme and varying concentrations of G6P and NDP-glucose to determine kinetic parameters.

The effect of trehalose and T6P as feedback inhibitors, and G1P, F6P, F16BP, CHES, 2PG, 3PG, cAMP and 2OG as allosteric regulators, was tested in the conditions described above but with fixed concentrations of G6P and ADP-glucose (both 0.3 mM). The same conditions were used to test possible allosteric regulators for wild type OtsA and mutants Arg213Glu and Arg384Glu. All experiments were performed in triplicate in a PheraStar plate reader (BMG Labtech) and data was analysed with Prism 5 (Graphpad Software).

To assess the inhibitory effect of ADP and allosteric effect of phosphoenolpyruvate an end-point assay was performed instead. Reactions (100 µl) containing 50 mM TRIS pH 7.5, 200 mM NaCl, 10 mM $MgCl_2$, 50 mM KCl, 4 µM *Mtr*OtsA, 0.3 mM ADP-glucose, 0.3 mM G6P and varying concentrations of ADP and PEP were incubated at 37 ºC and stopped at different time points with 10 µl of 1 M HCl, incubated for 1 minute and neutralized with NaOH. The reactions were diluted with 100 µl acetonitrile and run at 25 ºC on a Waters I-class UHPLC with a PDA detector (258 nm) using a ACQUITY UHPLC BEH Amide column (2.1 x 100 mm, 1.7 µm). Gradient elution (delivered at 0.13 mL/min) was employed using 80/20 acrilamide/water with 0.1 % NH_2OH (A) and water with 0.1 % NH_2OH (B) which started at 90 % A and decreased linearly to 55 % A over 10 min.

Isothermal Titration Calorimetry

Binding interaction between OtsA and ligands was characterized at 25 ºC, using a Microcal ITC200 titration calorimeter (Microcal). OtsA concentration of 60 µM was used for all titrations. Ligands (1 mM) were injected in 2ul aliquots. Titration data was recorded in 20mM TRIS pH 7.5, 500mM NaCl. Data was analysed by fitting a simple single-site model using Origin software (Microcal).

Acknowledgements

This work was funded by Bill & Melinda Gates Foundation (subcontract by the Foundation for the National Institutes of Health - NIH) (OPP1024021). VM would like to acknowledge Fundação para a Ciência e a Tecnologia for a postdoctoral fellowship (SFRH/BPD/79531/2011) and Bill & Melinda Gates Foundation HIT-TB (OPP1024021) and SHORTEN-TB (OPP1158806) for funding. MAGE is funded by the Cystic Fibrosis Trust Strategic Research Centre Award (RG77600). TLB received funding from the Wellcome Trust for facilities and support.

References

1. Nobre, A., Alarico, S., Maranha, A., Mendes, V., and Empadinhas, N. (2014) The molecular biology of mycobacterial trehalose in the quest for advanced tuberculosis therapies. *Microbiology* **160**, 1547-1570
2. Iturriaga, G., Suarez, R., and Nova-Franco, B. (2009) Trehalose metabolism: from osmoprotection to signaling. *Int J Mol Sci* **10**, 3793-3810
3. Webb, K. M., and DiRuggiero, J. (2012) Role of Mn2+ and compatible solutes in the radiation resistance of thermophilic bacteria and archaea. *Archaea* **2012**, 845756
4. Singer, M. A., and Lindquist, S. (1998) Thermotolerance in Saccharomyces cerevisiae: the Yin and Yang of trehalose. *Trends Biotechnol* **16**, 460-468
5. Lu, H., Zhu, Z., Dong, L., Jia, X., Sun, X., Yan, L., Chai, Y., Jiang, Y., and Cao, Y. (2011) Lack of trehalose accelerates H2O2-induced Candida albicans apoptosis through regulating Ca2+ signaling pathway and caspase activity. *PLoS ONE* **6**, e15808
6. Lee, J., Lin, E. W., Lau, U. Y., Hedrick, J. L., Bat, E., and Maynard, H. D. (2013) Trehalose Glycopolymers as Excipients for Protein Stabilization. *Biomacromolecules* **14**, 2561-2569
7. Kandror, O., DeLeon, A., and Goldberg, A. L. (2002) Trehalose synthesis is induced upon exposure of Escherichia coli to cold and is essential for viability at low temperatures. *Proceedings of the National Academy of Sciences of the United States of America* **99**, 9727-9732
8. Cardoso, F. S., Castro, R. F., Borges, N., and Santos, H. (2007) Biochemical and genetic characterization of the pathways for trehalose metabolism in Propionibacterium freudenreichii, and their role in stress response. *Microbiology* **153**, 270-280
9. Tapia, H., and Koshland, D. E. (2014) Trehalose is a versatile and long-lived chaperone for desiccation tolerance. *Current biology : CB* **24**, 2758-2766
10. Thevelein, J. M. (1984) Regulation of trehalose mobilization in fungi. *Microbiol Rev* **48**, 42-59
11. Elbein, A. D. (1974) The metabolism of alpha,alpha-trehalose. *Advances in carbohydrate chemistry and biochemistry* **30**, 227-256
12. Elbein, A. D., Pan, Y. T., Pastuszak, I., and Carroll, D. (2003) New insights on trehalose: a multifunctional molecule. *Glycobiology* **13**, 17R-27R
13. Djonovic, S., Urbach, J. M., Drenkard, E., Bush, J., Feinbaum, R., Ausubel, J. L., Traficante, D., Risech, M., Kocks, C., Fischbach, M. A., Priebe, G. P., and Ausubel, F. M. (2013) Trehalose biosynthesis promotes Pseudomonas aeruginosa pathogenicity in plants. *PLoS Pathog* **9**, e1003217
14. Wahl, V., Ponnu, J., Schlereth, A., Arrivault, S., Langenecker, T., Franke, A., Feil, R., Lunn, J. E., Stitt, M., and Schmid, M. (2013) Regulation of flowering by trehalose-6-phosphate signaling in Arabidopsis thaliana. *Science* **339**, 704-707
15. O'Hara, L. E., Paul, M. J., and Wingler, A. (2013) How do sugars regulate plant growth and development? New insight into the role of trehalose-6-phosphate. *Molecular plant* **6**, 261-274
16. Paul, M. J., Primavesi, L. F., Jhurreea, D., and Zhang, Y. (2008) Trehalose metabolism and signaling. *Annu Rev Plant Biol* **59**, 417-441
17. Fraenkel, D., and Nielsen, J. (2016) Trehalose-6-phosphate synthase and stabilization of yeast glycolysis. *FEMS Yeast Res* **16**, fov100
18. Deroover, S., Ghillebert, R., Broeckx, T., Winderickx, J., and Rolland, F. (2016) Trehalose-6-phosphate synthesis controls yeast gluconeogenesis downstream and independent of SNF1. *FEMS Yeast Res* **16**

19. Williams, B., Njaci, I., Moghaddam, L., Long, H., Dickman, M. B., Zhang, X., and Mundree, S. (2015) Trehalose Accumulation Triggers Autophagy during Plant Desiccation. *PLoS genetics* **11**, e1005705
20. Rubinsztein, D. C., Bento, C. F., and Deretic, V. (2015) Therapeutic targeting of autophagy in neurodegenerative and infectious diseases. *J Exp Med* **212**, 979-990
21. Welsh, K. J., Hunter, R. L., and Actor, J. K. (2013) Trehalose 6,6'-dimycolate--a coat to regulate tuberculosis immunopathogenesis. *Tuberculosis (Edinb)* **93 Suppl**, S3-9
22. Boot, M., van Winden, V. J. C., Sparrius, M., van de Weerd, R., Speer, A., Ummels, R., Rustad, T., Sherman, D. R., and Bitter, W. (2017) Cell envelope stress in mycobacteria is regulated by the novel signal transduction ATPase IniR in response to trehalose. *PLoS genetics* **13**, e1007131
23. Avonce, N., Mendoza-Vargas, A., Morett, E., and Iturriaga, G. (2006) Insights on the evolution of trehalose biosynthesis. *BMC Evol Biol* **6**, 109
24. Zaparty, M., Hagemann, A., Brasen, C., Hensel, R., Lupas, A. N., Brinkmann, H., and Siebers, B. (2013) The first prokaryotic trehalose synthase complex identified in the hyperthermophilic crenarchaeon Thermoproteus tenax. *PLoS ONE* **8**, e61354
25. Murphy, H. N., Stewart, G. R., Mischenko, V. V., Apt, A. S., Harris, R., McAlister, M. S., Driscoll, P. C., Young, D. B., and Robertson, B. D. (2005) The OtsAB pathway is essential for trehalose biosynthesis in Mycobacterium tuberculosis. *J Biol Chem* **280**, 14524-14529
26. Korte, J., Alber, M., Trujillo, C. M., Syson, K., Koliwer-Brandl, H., Deenen, R., Kohrer, K., DeJesus, M. A., Hartman, T., Jacobs, W. R., Jr., Bornemann, S., Ioerger, T. R., Ehrt, S., and Kalscheuer, R. (2016) Trehalose-6-Phosphate-Mediated Toxicity Determines Essentiality of OtsB2 in Mycobacterium tuberculosis In Vitro and in Mice. *PLoS Pathog* **12**, e1006043
27. Errey, J. C., Lee, S. S., Gibson, R. P., Martinez Fleites, C., Barry, C. S., Jung, P. M., O'Sullivan, A. C., Davis, B. G., and Davies, G. J. (2010) Mechanistic insight into enzymatic glycosyl transfer with retention of configuration through analysis of glycomimetic inhibitors. *Angew Chem Int Ed Engl* **49**, 1234-1237
28. Gibson, R. P., Turkenburg, J. P., Charnock, S. J., Lloyd, R., and Davies, G. J. (2002) Insights into trehalose synthesis provided by the structure of the retaining glucosyltransferase OtsA. *Chem Biol* **9**, 1337-1346
29. Miao, Y., Tenor, J. L., Toffaletti, D. L., Maskarinec, S. A., Liu, J., Lee, R. E., Perfect, J. R., and Brennan, R. G. (2017) Structural and In Vivo Studies on Trehalose-6-Phosphate Synthase from Pathogenic Fungi Provide Insights into Its Catalytic Mechanism, Biological Necessity, and Potential for Novel Antifungal Drug Design. *MBio* **8**
30. Asencion Diez, M. D., Miah, F., Stevenson, C. E., Lawson, D. M., Iglesias, A. A., and Bornemann, S. (2017) The Production and Utilization of GDP-glucose in the Biosynthesis of Trehalose 6-Phosphate by Streptomyces venezuelae. *J Biol Chem* **292**, 945-954
31. Jiang, Y., Chen, X. M., Liu, Y. J., Li, Y. T., Zhang, H. H., Dyson, P., Sheng, H. M., and An, L. Z. (2010) The catalytic efficiency of trehalose-6-phosphate synthase is effected by the N-loop at low temperatures. *Arch Microbiol* **192**, 937-943
32. Gibson, R. P., Tarling, C. A., Roberts, S., Withers, S. G., and Davies, G. J. (2004) The donor subsite of trehalose-6-phosphate synthase: binary complexes with UDP-glucose and UDP-2-deoxy-2-fluoro-glucose at 2 A resolution. *J Biol Chem* **279**, 1950-1955
33. Pan, Y. T., Carroll, J. D., and Elbein, A. D. (2002) Trehalose-phosphate synthase of Mycobacterium tuberculosis. Cloning, expression and properties of the recombinant enzyme. *Eur J Biochem* **269**, 6091-6100
34. Chen, X., An, L., Fan, X., Ju, F., Zhang, B., Sun, H., Xiao, J., Hu, W., Qu, T., Guan, L., Tang, S., Chen, T., Liu, G., and Dyson, P. (2017) A trehalose biosynthetic enzyme doubles as an osmotic stress sensor to regulate bacterial morphogenesis. *PLoS genetics* **13**, e1007062
35. Asencion Diez, M. D., Demonte, A. M., Syson, K., Arias, D. G., Gorelik, A., Guerrero, S. A., Bornemann, S., and Iglesias, A. A. (2015) Allosteric regulation of the partitioning of

glucose-1-phosphate between glycogen and trehalose biosynthesis in Mycobacterium tuberculosis. *Biochim Biophys Acta* **1850**, 13-21
36. Killick, K. A. (1979) Trehalose 6-phosphate synthase from Dictyostelium discoideum: partial purification and characterization of the enzyme from young sorocarps. *Arch Biochem Biophys* **196**, 121-133
37. Silva, Z., Alarico, S., and da Costa, M. S. (2005) Trehalose biosynthesis in Thermus thermophilus RQ-1: biochemical properties of the trehalose-6-phosphate synthase and trehalose-6-phosphate phosphatase. *Extremophiles* **9**, 29-36
38. Pires, D. E., Blundell, T. L., and Ascher, D. B. (2016) mCSM-lig: quantifying the effects of mutations on protein-small molecule affinity in genetic disease and emergence of drug resistance. *Sci Rep* **6**, 29575
39. Londesborough, J., and Vuorio, O. E. (1993) Purification of trehalose synthase from baker's yeast. Its temperature-dependent activation by fructose 6-phosphate and inhibition by phosphate. *Eur J Biochem* **216**, 841-848
40. Hu, P., Janga, S. C., Babu, M., Diaz-Mejia, J. J., Butland, G., Yang, W., Pogoutse, O., Guo, X., Phanse, S., Wong, P., Chandran, S., Christopoulos, C., Nazarians-Armavil, A., Nasseri, N. K., Musso, G., Ali, M., Nazemof, N., Eroukova, V., Golshani, A., Paccanaro, A., Greenblatt, J. F., Moreno-Hagelsieb, G., and Emili, A. (2009) Global functional atlas of Escherichia coli encompassing previously uncharacterized proteins. *PLoS biology* **7**, e96
41. Huergo, L. F., and Dixon, R. (2015) The Emergence of 2-Oxoglutarate as a Master Regulator Metabolite. *Microbiol Mol Biol Rev* **79**, 419-435
42. Zheng, L., Zhou, X., Zhang, H., Ji, X., Li, L., Huang, L., and Bai, L. (2012) Structural and functional analysis of validoxylamine A 7'-phosphate synthase ValL involved in validamycin A biosynthesis. *PLoS ONE* **7**, e32033
43. Cavalier, M. C., Yim, Y. S., Asamizu, S., Neau, D., Almabruk, K. H., Mahmud, T., and Lee, Y. H. (2012) Mechanistic Insights into Validoxylamine A 7 '-Phosphate Synthesis by VldE Using the Structure of the Entire Product Complex. *PLoS ONE* **7**
44. Chandra, G., Chater, K. F., and Bornemann, S. (2011) Unexpected and widespread connections between bacterial glycogen and trehalose metabolism. *Microbiology* **157**, 1565-1572
45. Leiba, J., Syson, K., Baronian, G., Zanella-Cleon, I., Kalscheuer, R., Kremer, L., Bornemann, S., and Molle, V. (2013) Mycobacterium tuberculosis maltosyltransferase GlgE, a genetically validated antituberculosis target, is negatively regulated by Ser/Thr phosphorylation. *J Biol Chem* **288**, 16546-16556
46. Trevisol, E. T., Panek, A. D., De Mesquita, J. F., and Eleutherio, E. C. (2014) Regulation of the yeast trehalose-synthase complex by cyclic AMP-dependent phosphorylation. *Biochim Biophys Acta* **1840**, 1646-1650
47. Sengupta, S., Banerjee, S., Lahiri, S., Dutta, T., Dhar, T. K., and Ghosh, A. K. (2014) Purification, characterization, sequencing and molecular cloning of a novel cysteine methyltransferase that regulates trehalose-6-phosphate synthase from Saccharomyces cerevisiae. *Biochim Biophys Acta* **1840**, 1861-1871
48. Bennett, B. D., Kimball, E. H., Gao, M., Osterhout, R., Van Dien, S. J., and Rabinowitz, J. D. (2009) Absolute metabolite concentrations and implied enzyme active site occupancy in Escherichia coli. *Nat Chem Biol* **5**, 593-599
49. Albe, K. R., Butler, M. H., and Wright, B. E. (1990) Cellular concentrations of enzymes and their substrates. *J Theor Biol* **143**, 163-195
50. Leslie, A. G. W., and Powell, H. R. (2007) Processing diffraction data with MOSFLM. *Nato Sci Ser Ii Math* **245**, 41-51
51. Evans, P. R., and Murshudov, G. N. (2013) How good are my data and what is the resolution? *Acta Crystallogr D* **69**, 1204-1214
52. Winn, M. D., Ballard, C. C., Cowtan, K. D., Dodson, E. J., Emsley, P., Evans, P. R., Keegan, R. M., Krissinel, E. B., Leslie, A. G., McCoy, A., McNicholas, S. J., Murshudov, G. N., Pannu,

N. S., Potterton, E. A., Powell, H. R., Read, R. J., Vagin, A., and Wilson, K. S. (2011) Overview of the CCP4 suite and current developments. *Acta Crystallogr D Biol Crystallogr* **67**, 235-242

53. Vonrhein, C., Flensburg, C., Keller, P., Sharff, A., Smart, O., Paciorek, W., Womack, T., and Bricogne, G. (2011) Data processing and analysis with the autoPROC toolbox. *Acta Crystallogr D Biol Crystallogr* **67**, 293-302
54. McCoy, A. J., Grosse-Kunstleve, R. W., Adams, P. D., Winn, M. D., Storoni, L. C., and Read, R. J. (2007) Phaser crystallographic software. *Journal of applied crystallography* **40**, 658-674
55. Adams, P. D., Afonine, P. V., Bunkoczi, G., Chen, V. B., Davis, I. W., Echols, N., Headd, J. J., Hung, L. W., Kapral, G. J., Grosse-Kunstleve, R. W., McCoy, A. J., Moriarty, N. W., Oeffner, R., Read, R. J., Richardson, D. C., Richardson, J. S., Terwilliger, T. C., and Zwart, P. H. (2010) PHENIX: a comprehensive Python-based system for macromolecular structure solution. *Acta Crystallogr D Biol Crystallogr* **66**, 213-221
56. Emsley, P., Lohkamp, B., Scott, W. G., and Cowtan, K. (2010) Features and development of Coot. *Acta Crystallogr D Biol Crystallogr* **66**, 486-501

Author contributions

VM designed the study. VM performed all structural work with contributions of MB. MAGE performed all the biochemical experiments. NV performed the biophysical experiments. VM wrote the manuscript with contributions from MA, MVBD and TLB. All authors reviewed and approved the manuscript.

Abbreviations

GlgE – Maltosyltransferase

Mak – Maltokinase

OtsA – Trehalose-6-phosphate synthase

OtsB2 – Trehalose-6-phosphate phosphatase

TreS – Trehalose synthase

TreY – Maltooligosyltrehalose synthase

TreZ – Maltooligosyltrehalose trehalohydrolase

2OG- 2-oxoglutarate

2PG – 2-phosphoglycerate

CHES - N-Cyclohexyl-2-aminoethanesulfonic acid

F16BP – fructose-1,6-biphosphate

F6P – fructose-6-phosphate

G1P – glucose-1-phosphate

G6P – glucose-6-phosphate

T6P – trehalose-6-phopshate

Author financial disclosure statement

The authors do not have financial or commercial competing interests.

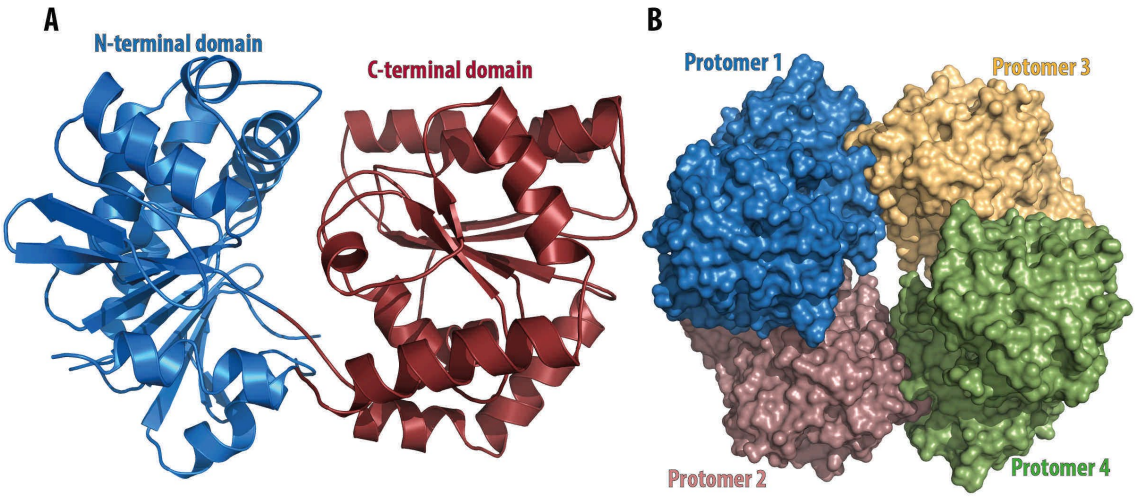

Figure 1: (A) Representation of the overall structure of *M. thermoresistibile* OtsA. The N-terminal domain consists of residues 1-247 and 462-486, the C-terminal domain of residues 248-461. View of *M. thermoresistibile* OtsA tetramer (B).

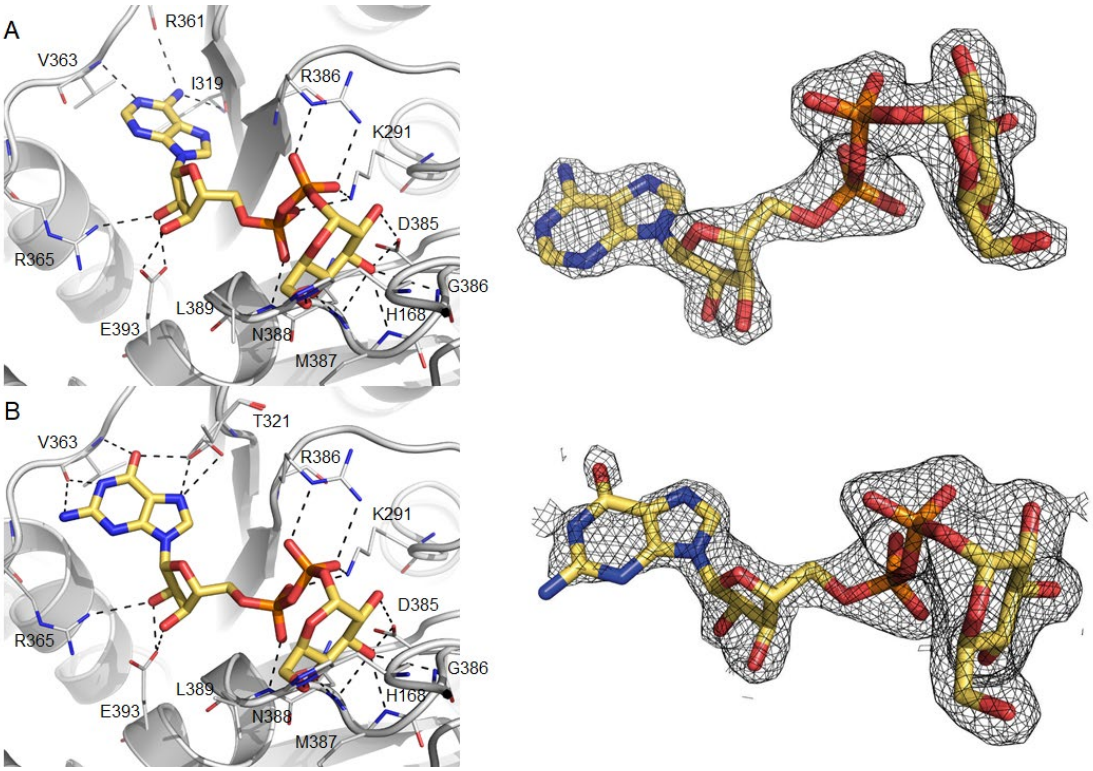

Figure 2: Detailed view of the active site of *M. thermoresistibile* OtsA with ADP-glucose (A) and with GDP-glucose bound (B) with "omit maps" shown.

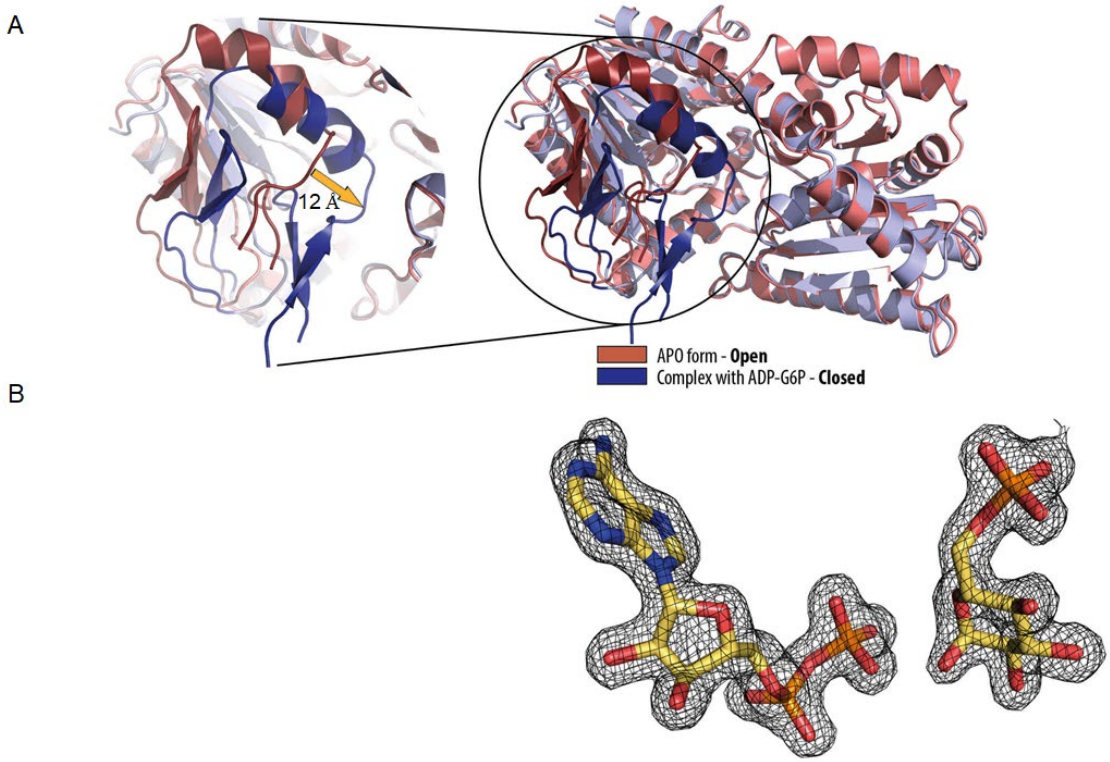

Figure 3: View of OtsA in an open (salmon and red) and closed conformation (violet and blue) and superposition of the two conformations. (B)Representation of the active site of *M. thermoresistibile* OtsA with ADP (white) and G6P (yellow) bound with "omit map" shown.

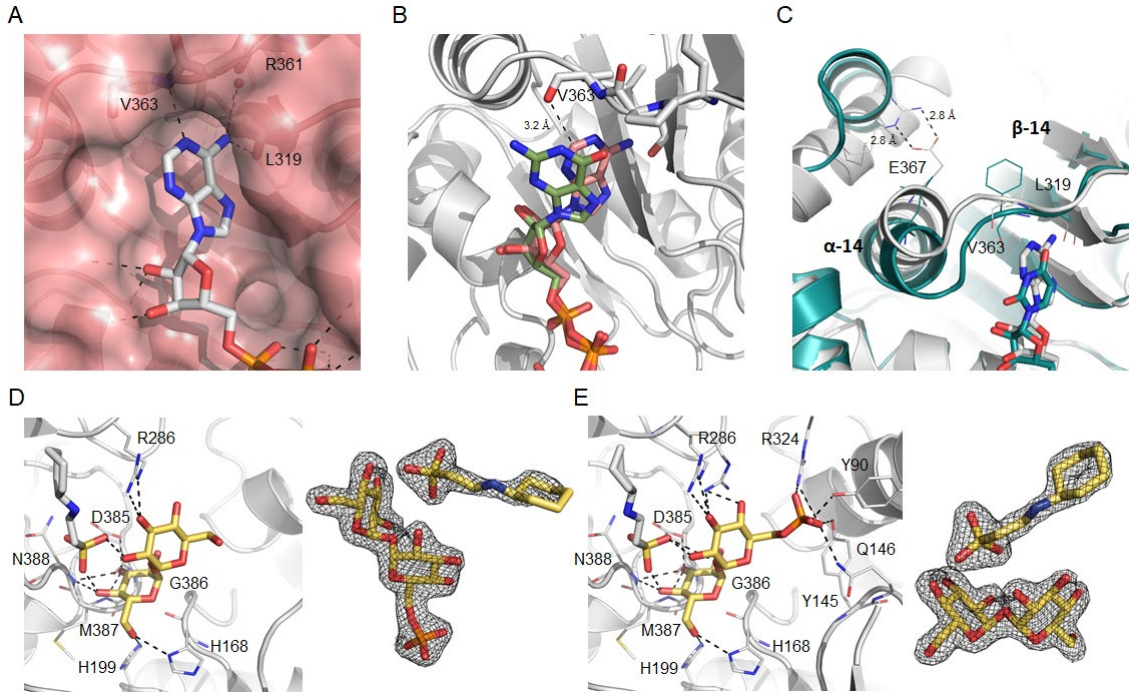

Figure 4: View of the binding site of the adenine moiety of ADP-glucose (A). Superposition of ADP-glucose and GDP-glucose structures (B). Superposition of *Mtr*OtsA structure with ADP-glucose bound and *E. coli* OtsA structure with UDP-glucose bound (PDB code: 1UQU) (C). Alpha helix 14 (α-14) and beta strand 14 (β-14) are shown. Detailed view of the active site of *M. thermoresistibile* OtsA with trehalose (D) and with T6P bound (E) with CHES visible in both structures. "Omit maps" are shown both trehalose, T6P and CHES.

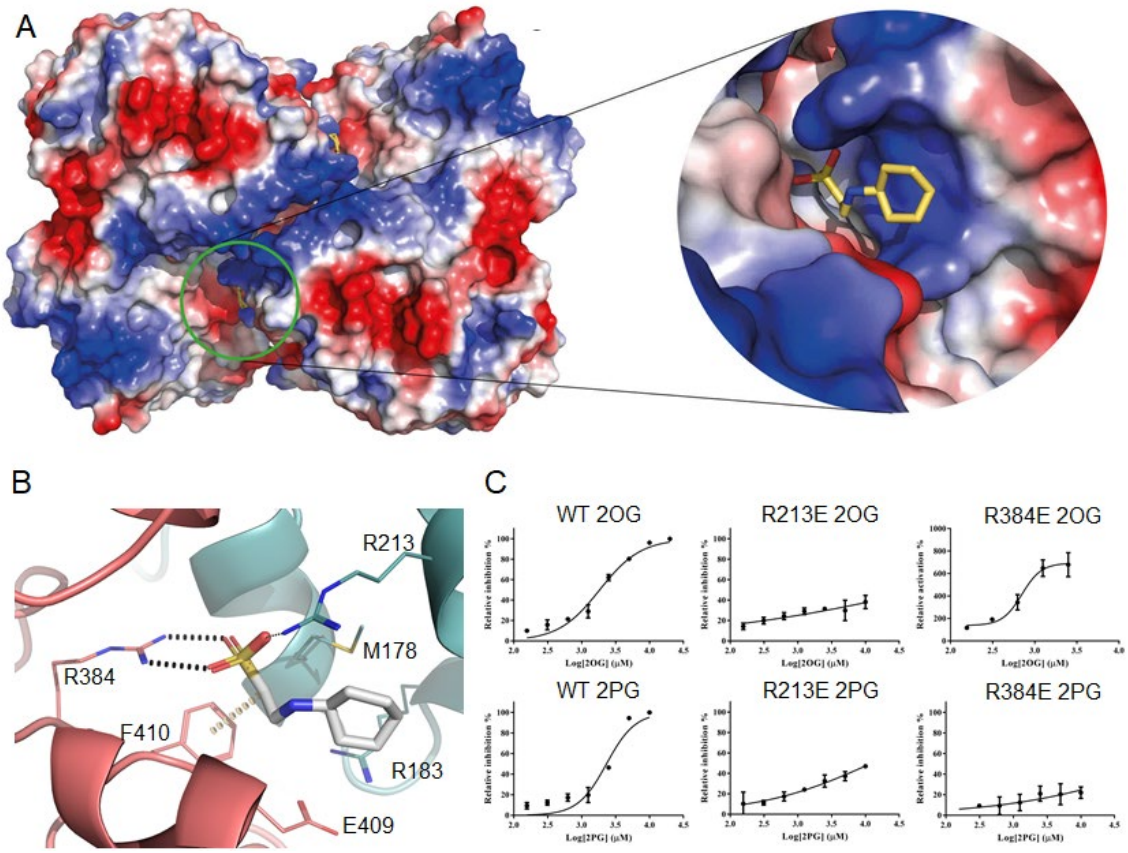

Figure 5: View of the allosteric site of *M. thermoresistibile* OtsA with CHES bound with protein surface electrostatic potential shown (A). Detailed view of the CHES binding site and its interactions with OtsA (B). The interactions were calculated with Arpeggio (http://structure.bioc.cam.ac.uk/arpeggio) using the apo structure (5JIJ). Black dots represent hydrogen bonds and yellow disks a carbon-π interaction. The two protomers are colored differently. (C) Activity profiles of *M. thermoresistibile* wild type OtsA and the allosteric site mutants Arg213Glu and Arg384Glu in the presence of the allosteric effectors 2OG and 2PG.

Table 1: Kinetic parameters of *M. thermoresistibile* OtsA.

	Substrate	K_m (mM)	k_{cat} (s^{-1})	k_{cat}/K_m
WT	ADP-Glucose	0.25 ± 0.02	26 ± 1	104 ± 13
	GDP-Glucose	0.29 ± 0.02	5.1 ± 0.2	18 ± 2
	UDP-Glucose	1.7 ± 0.1	36 ± 1	21 ± 2
	Glucose-6P	3.3 ± 0.1	26 ± 1	7.9 ± 0.5
L319I	ADP-Glucose	0.71 ± 0.18	8.4 ± 0.7	12 ± 2
	GDP-Glucose	0.35 ± 0.04	3.1 ± 0.1	8.9 ± 1.4
	UDP-Glucose	1.4 ± 0.1	8.9 ± 0.4	6.4 ± 0.7
	Glucose-6P	3.3 ± 0.2	6.4 ± 0.2	1.9 ± 0.2
V363F	ADP-Glucose	0.60 ± 0.03	11 ± 1	18 ± 2
	GDP-Glucose	0.74 ± 0.08	14 ± 1	19 ± 3
	UDP-Glucose	0.68 ± 0.06	13 ± 1	19 ± 3
	Glucose-6P	3.1 ± 0.2	19 ± 1	6.1 ± 0.7
L319I, E367L	ADP-Glucose	0.63 ± 0.04	14 ± 1	22 ± 3
	GDP-Glucose	0.70 ± 0.05	9.2 ± 0.4	13 ± 2
	UDP-Glucose	0.63 ± 0.03	15 ± 1	24 ± 3
	Glucose-6P	3.7 ± 0.2	21 ± 1	5.7 ± 0.5
L319I, V363F, E367L	ADP-Glucose	1.3 ± 0.1	19 ± 1	15 ± 2
	GDP-Glucose	0.90 ± 0.06	16 ± 1	18 ± 2
	UDP-Glucose	0.52 ± 0.05	22 ± 1	42 ± 6
	Glucose-6P	3.2 ± 0.2	17 ± 1	5.3 ± 0.6
R213E	ADP-Glucose	0.31 ± 0.01	56 ± 2	180 ± 13
	Glucose-6P	3.3 ± 0.3	33 ± 2	10 ± 1
R384E	ADP-Glucose	1.9 ± 0.2	3.2 ± 0.1	1.7 ± 0.2
	Glucose-6P	2.9 ± 0.2	2.1 ± 0.2	0.77 ± 0.05

Table 2: Effect of allosteric regulators and feedback inhibitors in *M. thermoresistibile* OtsA activity. Values are in (mM) and 95% confidence intervals are given in brackets.

	WT	**R213E**	**R384E**
2OG	IC_{50} = 1.8 (1.6-2.1)	IC_{50} = 73 (18-302)	EC_{50} = 0.70 (0.56-0.88)
2PG	IC_{50} = 2.3 (2.0-2.7)	IC_{50} = 12 (6.3-24)	IC_{50} < 100